Supplementary Materials for

Highly tunable quadruple quantum dot in a narrow bandgap semiconductor InAs nanowire

Jingwei Mu,[a,c] Shaoyun Huang,[a] Zhi-Hai Liu,[a] Weijie Li,[a,c] Ji-Yin Wang,[a] Dong Pan,[b] Guang-Yao Huang,[a] Yuanjie Chen,[a] Jianhua Zhao,[b,d,†] and H. Q. Xu[a,c,d,*]

[a]*Beijing Key Laboratory of Quantum Devices, Key Laboratory for the Physics and Chemistry of Nanodevices and Department of Electronics, Peking University, Beijing 100871, China*

[b]*State Key Laboratory of Superlattices and Microstructures, Institute of Semiconductors, Chinese Academy of Sciences, P.O. Box 912, Beijing 100083, China*

[c]*Academy for Advanced Interdisciplinary Studies, Peking University, Beijing 100871, China*

[d]*Beijing Academy of Quantum Information Sciences, Beijing 100193, China*

Corresponding authors. Emails: [*]hqxu@pku.edu.cn; [†]jhzhao@semi.ac.cn

(January 18, 2020)

Outline

I. Charge stability diagram of a single QD defined in the InAs nanowire

II. Complementary measurements of the QQD device studied in the main article

III. Verification of the current lines that arise from resonant transport through QD2 and QD4 in the QQD device studied in the main article

IV. Electrostatic capacitance network model for the QQD device studied in the main article

V. Achieving the resonance between the energy levels of QD3 and QD4 in the QQD device studied in the main article

I. Charge stability diagram of a single QD defined in the InAs nanowire

Figure S1 displays the differential conductance dI_{ds}/dV_{ds} of a single quantum dot (QD) defined in the InAs nanowire as a function of source-drain bias voltage V_{ds} and voltage V_{G4} applied to plunger gate G4 (charge stability diagram). Here, gates G3 and G5 are used to define the two tunneling barriers of the single QD. The regular Coulomb diamonds as well as the close points seen at a zero V_{ds} between neighboring Coulomb diamonds indicate the formation of a single QD. The small electron effective mass of InAs, $m_e^*=0.23m_e$, leads to strong quantum confinement effect[1] and QDs built from InAs nanowires can easily possess a large energy level separation. Thus, a quantization energy of ~1.5 meV is observed in the measured charge stability diagram of the single QD. Besides, we also extract an electrostatic charging energy of E_C~5 meV, determined by the Coulomb interaction of the additional electron with other electrons in the QD from the charge stability diagram.

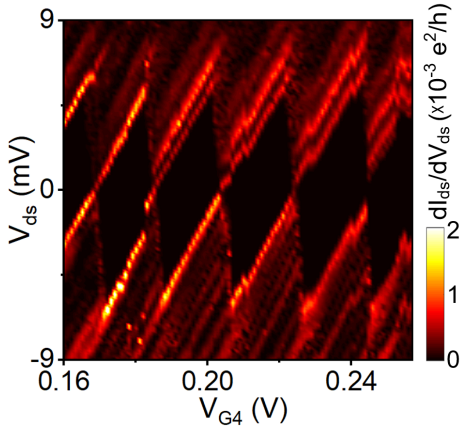

Fig. S1 Differential conductance dI_{ds}/dV_{ds} of a single QD defined in the InAs nanowire as a function of source-drain bias voltage V_{ds} and gate voltage V_{G4}. Here, the single QD is defined by setting the voltages applied to gates G3 and G5 at $V_{G3}=-2.85$ V and $V_{G5}=-3.5$ V, see Fig. 1 in the main article for the device structure and the measurement circuit setup.

II. Complementary measurements of the QQD device studied in the main article

Figure S2 shows the source-drain current I_{ds} measured for the quadruple quantum dot (QQD) defined in the InAs nanowire (see Fig. 1 in the main article) at V_{ds} = 0.1 mV as a function of voltages V_{G4} and V_{G6} applied to plunger gates G4 and G6 [Fig. S2(a)], and as a function of voltages V_{G4} and V_{G8} applied to plunger gates G4 and G8 [Fig. S2(b)]. Both charge stability diagrams show the similar characteristics of a double QD (DQD), i.e., only two groups of resonant current lines of different slopes are present in each of the two charge stability diagrams.[2] Thus, we can infer that the current lines in Fig. S2(a) [Fig. S2(b)] arise from resonant electron

transport through QD2 and QD3 (QD2 and QD4), and plunger gates G4, G6 and G8 couple strongly to their locally addressed QDs but weakly to the other QDs. In other words, the parasitical capacitances between a plunger gate and QDs other than its locally addressed one are very small in the QQD device. Therefore, it is difficult to map out the complete charge state configuration of the QQD in a two-dimensional charge stability diagram effectively by scanning plunger gates. This is the reason why in the main article a two-dimensional charge stability diagram of the QQD is measured and plotted as a function of gate voltages V_{G3} and V_{G7}. It is important to note that, in Fig. S2(b), no recognizable avoiding crossing of two current lines of different slopes is found, due to the weak direct coupling between QD2 and QD4, which are separated by QD3.

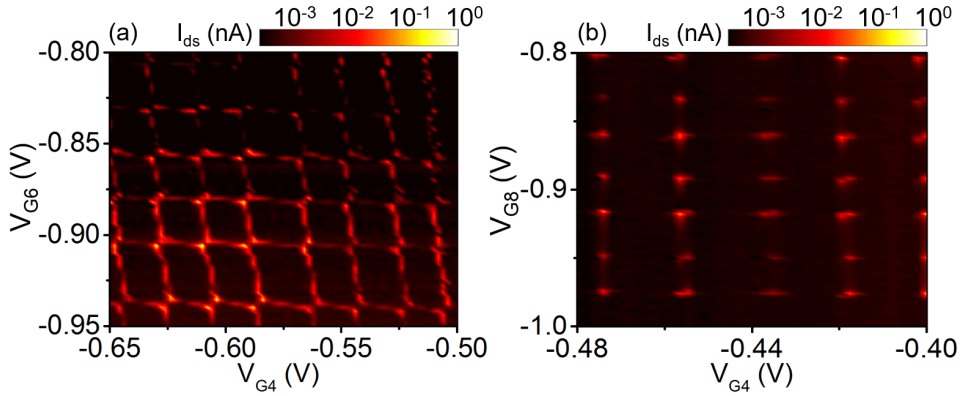

Fig. S2 (a) Source-drain current I_{ds} measured at V_{ds} = 0.1 mV for the QQD device defined in the InAs nanowire as shown in Fig. 1 of the main article as a function of voltages V_{G4} and V_{G6} applied to plunger gates G4 and G6, while setting the voltage applied to plunger gate G8 at V_{G8} = −1 V. (b) the same as (a) but measured as a function of voltages V_{G4} and V_{G8} applied to plunger gates G4 and G8, while setting the voltage applied to plunger gate G6 at V_{G6} = −0.6 V. The QQD is defined in the InAs nanowire with the voltages applied to barrier gates G1, G3, G5, G7, and G9 set at V_{G1} = −2.545 V, V_{G3} = −2.74 V, V_{G5} = −3.39 V, V_{G7} = −3.65 V, and V_{G9} = −3.845 V, respectively. Plunger gate G2 is unused and is left floating throughout the measurements.

III. Verification of the current lines that arise from resonant transport through QD2 and QD4 in the QQD device studied in the main article

Plunger gate G8 possesses a strong coupling to its locally addressed QD4 but relatively weak cross-talks to the other QDs. We, therefore, tune the voltage V_{G8} applied to plunger gate G8 and examine the changes of current lines in the measured charge stability diagrams shown in Fig. S3(a) and S3(b). Here, we observe that the positions of the current lines in groups 1, 2 and 3 remain approximately unchanged, while the positions of the current lines in group 4 move toward

the positive direction of V_{G7}, when the voltage V_{G8} is tuned from $V_{G8} = -0.94$ V to $V_{G8} = -0.95$ V. Thus, the current lines in group 4 evidently arise from resonant electron transport through QD4. It should be noted that a current line in group 3, marked by P in Fig. S3(a), moves noticeably also towards the positive direction of V_{G7}. This is because an energy level of QD4 gradually approaches the energy level of QD3 represented by current line P and pushes the energy level to move due to level repulsion with decreasing V_{G8}. In the same way, the assignment of the current lines in group 2 as arising from resonant transport through QD2 is double-checked by tuning the voltage V_{G4} applied to plunger gate G4 from $V_{G4} = -0.380$ V to $V_{G4} = -0.385$ V and examining the changes of current lines in the measured charge stability diagrams as shown in Fig. S3(c) and S3(d). Clearly, it is seen that the current lines in group 2 move significantly towards the positive direction of V_{G3} and all the other current lines remain approximately unchanged with decreasing V_{G4}, confirming our previous assignment for the current lines in group 2.

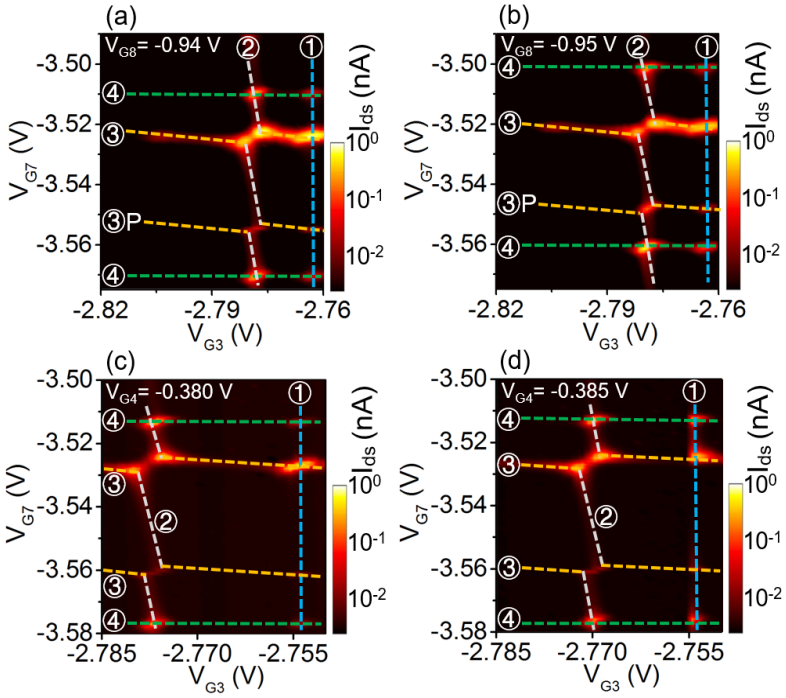

Fig. S3 (a) and (b) Source-drain current I_{ds} measured for the InAs nanowire QQD as shown in Fig. 1 of the main article at V_{ds} = 0.2 mV as a function of V_{G3} and V_{G7} at two different values of plunger gate voltage V_{G8}. Here, to define the InAs nanowire QQD, the voltages applied to barrier gates G1, G5, and G9 are set at $V_{G1} = -2.538$ V, $V_{G5} = -3.35$ V, and $V_{G9} = -3.855$ V, and the voltages applied to plunger gates G4 and G6 are set at $V_{G4} = -0.38$ V and $V_{G6} = -1.05$ V. (c) and (d) The same as (a) and (b) but for the measurements at V_{ds} = 0.1 mV and at two different values of V_{G4}. Here, the QQD is defined by setting the voltages applied to barrier gates G1, G5, and G9

at V_{G1} = −2.55 V, V_{G5} = −3.35 V, and V_{G9} = −3.855 V, and the voltages applied to plunger gates G6 and G8 at V_{G6} = −1.05 V and V_{G8} = −0.94 V.

IV. Electrostatic capacitance network model for the QQD device studied in the main article

Electrostatic capacitance network models have been successfully employed to describe the characteristics of the charge stability diagrams of a DQD and a Triple QD (TQD).[2-5] Here, we present an electrostatic capacitance network model for the InAs nanowire QQD studied in the main article. In our work, the charge stability diagrams of the QQD are measured at different voltages V_{G4} and V_{G6} as a function of V_{G3} and V_{G7} (cf. Fig. 1 in the main article). The QQD device can modeled by a circuit shown in Fig. 4(a) of the main article, which includes the source and drain electrodes, four gates (G3, G4, G6 and G7) that are changed in the measurements, and four QDs (QD1, QD2, QD3 and QD4) that act as four nodes and marked with colored ovals in the model circuit. Based on the classical theory, the charges on individual QDs can be expressed in terms of relevant gate voltages and capacitances as,

$$
\begin{aligned}
Q_{QD1} &= C_S(V_{QD1}-V_S)+C_{G3\text{-}QD1}(V_{QD1}-V_{G3})+C_{M12}(V_{QD1}-V_{QD2})+C_{M13}(V_{QD1}-V_{QD3}),\\
Q_{QD2} &= C_{M12}(V_{QD2}-V_{QD1})+C_{G3\text{-}QD2}(V_{QD2}-V_{G3})+C_{G4\text{-}QD2}(V_{QD2}-V_{G4})+C_{G7\text{-}QD2}(V_{QD2}-V_{G7})\\
&\quad +C_{M23}(V_{QD2}-V_{QD3})+C_{M24}(V_{QD2}-V_{QD4}),\\
Q_{QD3} &= C_{M23}(V_{QD3}-V_{QD2})+C_{G6\text{-}QD3}(V_{QD3}-V_{G6})+C_{G7\text{-}QD3}(V_{QD3}-V_{G7})+C_{G3\text{-}QD3}(V_{QD3}-V_{G3})\\
&\quad +C_{M13}(V_{QD3}-V_{QD1})+C_{M34}(V_{QD3}-V_{QD4}),\\
Q_{QD4} &= C_{M34}(V_{QD4}-V_{QD3})+C_{G7\text{-}QD4}(V_{QD4}-V_{G7})+C_{M24}(V_{QD4}-V_{QD2})+C_D(V_{QD4}-V_D).
\end{aligned}
\tag{1}
$$

Defining the vectors

$$
\hat{V}_{QD}=\{V_{QD1},V_{QD2},V_{QD3},V_{QD4}\}^T,\quad \hat{V}_G=\{V_S,V_{G3},V_{G4},V_{G6},V_{G7},V_D\}^T,\quad \hat{Q}_{QD}=\{Q_1,Q_2,Q_3,Q_4\}^T,
$$

Eq. (1) can be written as

$$
\hat{Q}_{QD}=C_{QD}\cdot\hat{V}_{QD}+C_{QD\text{-}G}\cdot\hat{V}_G, \tag{2}
$$

with matrices C_{QD} and $C_{QD\text{-}G}$ given by

$$
C_{QD}=\begin{pmatrix} C_1 & -C_{M12} & -C_{M13} & 0\\ -C_{M12} & C_2 & -C_{M23} & -C_{M24}\\ -C_{M13} & -C_{M23} & C_3 & -C_{M34}\\ 0 & -C_{M24} & -C_{M34} & C_4 \end{pmatrix}, \tag{3}
$$

$$C_{QD\text{-}G} = \begin{pmatrix} -C_S & -C_{G3\text{-}QD1} & 0 & 0 & 0 & 0 \\ 0 & -C_{G3\text{-}QD2} & -C_{G4\text{-}QD2} & 0 & -C_{G7\text{-}QD2} & 0 \\ 0 & -C_{G3\text{-}QD3} & 0 & -C_{G6\text{-}QD3} & -C_{G7\text{-}QD3} & 0 \\ 0 & 0 & 0 & 0 & -C_{G7\text{-}QD4} & -C_D \end{pmatrix}, \tag{4}$$

where

$$\begin{aligned} C_1 &= C_S + C_{G3\text{-}QD1} + C_{M12} + C_{M13}, \\ C_2 &= C_{M12} + C_{G3\text{-}QD2} + C_{G4\text{-}QD2} + C_{M23} + C_{M24} + C_{G7\text{-}QD2}, \\ C_3 &= C_{M23} + C_{G6\text{-}QD3} + C_{G7\text{-}QD3} + C_{M13} + C_{M34} + C_{G3\text{-}QD3}, \\ C_4 &= C_{M34} + C_{G7\text{-}QD4} + C_{M24} + C_D. \end{aligned} \tag{5}$$

Then, the electric potentials on the QDs can be calculated from

$$\hat{V}_{QD} = C_{QD}^{-1}\left(\hat{Q}_{QD} - C_{QD\text{-}G}\cdot\hat{V}_G\right), \tag{6}$$

and the electrostatic energy of the QQD reads

$$\begin{aligned} E &= \frac{1}{2}\hat{V}_{QD}^T\cdot C_{QD}\cdot\hat{V}_{QD} \\ &= \frac{1}{2}\hat{V}_{QD}^T\left(\hat{Q}_{QD} - C_{QD\text{-}G}\cdot\hat{V}_G\right) \\ &= \frac{1}{2}\left(\hat{Q}_{QD} - C_{QD\text{-}G}\cdot\hat{V}_G\right)^T[C_{QD}^{-1}]^T\left(\hat{Q}_{QD} - C_{QD\text{-}G}\cdot\hat{V}_G\right). \end{aligned} \tag{7}$$

Because $Q_i = -eN_i$ (i = 1, 2, 3, 4), the chemical potentials μ_i in individual QDs are given by

$$\begin{aligned} \mu_1(N_1,N_2,N_3,N_4,V_{G3},V_{G4},V_{G6},V_{G7}) &= E(N_1,N_2,N_3,N_4,V_{G3},V_{G4},V_{G6},V_{G7}) - E(N_1-1,N_2,N_3,N_4, \\ &\quad V_{G3},V_{G4},V_{G6},V_{G7}), \\ \mu_2(N_1,N_2,N_3,N_4,V_{G3},V_{G4},V_{G6},V_{G7}) &= E(N_1,N_2,N_3,N_4,V_{G3},V_{G4},V_{G6},V_{G7}) - E(N_1,N_2-1,N_3,N_4, \\ &\quad V_{G3},V_{G4},V_{G6},V_{G7}), \\ \mu_3(N_1,N_2,N_3,N_4,V_{G3},V_{G4},V_{G6},V_{G7}) &= E(N_1,N_2,N_3,N_4,V_{G3},V_{G4},V_{G6},V_{G7}) - E(N_1,N_2,N_3-1,N_4, \\ &\quad V_{G3},V_{G4},V_{G6},V_{G7}), \\ \mu_4(N_1,N_2,N_3,N_4,V_{G3},V_{G4},V_{G6},V_{G7}) &= E(N_1,N_2,N_3,N_4,V_{G3},V_{G4},V_{G6},V_{G7}) - E(N_1,N_2,N_3,N_4-1, \\ &\quad V_{G3},V_{G4},V_{G6},V_{G7}). \end{aligned} \tag{8}$$

The electron occupancies of the four QDs can be manipulated by adjusting the voltages of the plunger gates or barrier gates. For single electron tunneling through QDi to occur, the chemical potentials μ_i in QDi at occupancies N_i and N_i + 1 need to be equal. This can be achieved by

adjusting a set of selected gate voltages while keeping the other gate voltages unchanged. In our experiment, we have measured single electron tunneling as a function of V_{G3} and V_{G7} at fixed values for the other gate voltages. Therefore, the condition for the single electron tunneling through QD*i* to take place is given by

$$\mu_i(N_i, V_{G3}, V_{G7}) = \mu_i(N_i + 1, V_{G3}, V_{G7}). \tag{9}$$

In our experiment, we see that the current lines in each group, i.e., arising from resonant tunneling transport through a QD, are nearly parallel in the measured charge stability diagram of the QQD. Thus, the voltages differences $\Delta V_{G3\text{-}QDi}$ and $\Delta V_{G7\text{-}QDi}$, where $\Delta V_{G3\text{-}QDi}$ ($\Delta V_{G7\text{-}QDi}$) measures the distance in V_{G3} (V_{G7}) between two neighboring current lines in group i at a fixed value of V_{G7} (V_{G3}), can be written as,

$$\begin{aligned}
&\mu_i(N_i, V_{G3}, V_{G7}) = \mu_i(N_i + 1, V_{G3} + \Delta V_{G3\text{-}QDi}, V_{G7}) \\
&\mu_i(N_i, V_{G3}, V_{G7}) = \mu_i(N_i + 1, V_{G3}, V_{G7} + \Delta V_{G7\text{-}QDi}).
\end{aligned} \tag{10}$$

Note that, in the above equations, Eqs (9) and (10), we have omitted those occupancy numbers and gate voltages that have not been changed during the considered tunneling process. By solving Eq. (10) with the help of Eqs. (7) and (8), $\Delta V_{G3\text{-}QDi}$ and $\Delta V_{G7\text{-}QDi}$ can be obtained as,

$$\Delta V_{G3\text{-}QD1} = \frac{e}{C_{G3\text{-}QD1} + \frac{C_{M12}}{C_2} C_{G3\text{-}QD2} + (\frac{C_{M13}}{C_2} + \frac{C_{M12} C_{M23}}{C_2 C_3}) C_{G3\text{-}QD3}},$$

$$\Delta V_{G7\text{-}QD1} = \frac{e}{\frac{C_{M13}}{C_3} C_{G7\text{-}QD3} + (\frac{C_{M13}}{C_2} + \frac{C_{M12} C_{M23}}{C_2 C_3}) C_{G7\text{-}QD3}},$$

$$\Delta V_{G3\text{-}QD2} = \frac{e}{C_{G3\text{-}QD2} + \frac{C_{M12}}{C_1} C_{G3\text{-}QD1} + \frac{C_{M23}}{C_3} C_{G3\text{-}QD3}},$$

$$\Delta V_{G7\text{-}QD2} = \frac{e}{C_{G7\text{-}QD2} + \frac{C_{M23}}{C_3} C_{G7\text{-}QD3} + (\frac{C_{M24}}{C_4} + \frac{C_{M23} C_{M34}}{C_3 C_4}) C_{G7\text{-}QD4}},$$

$$\Delta V_{G3\text{-}QD3} = \frac{e}{C_{G3\text{-}QD3} + (\frac{C_{M13}}{C_1} + \frac{C_{M12} C_{M23}}{C_1 C_2}) C_{G3\text{-}QD1} + \frac{C_{M23}}{C_2} C_{G3\text{-}QD2}},$$

$$\Delta V_{G7\text{-}QD3} = \frac{e}{C_{G7\text{-}QD3} + \frac{C_{M34}}{C_4} C_{G7\text{-}QD4} + \frac{C_{M23}}{C_2} C_{G7\text{-}QD2}},$$

$$\Delta V_{G3\text{-}QD4} = \frac{e}{(\frac{C_{M24}}{C_2} + \frac{C_{M23}C_{M34}}{C_2C_3})C_{G3\text{-}QD2} + \frac{C_{M34}}{C_3}C_{G3\text{-}QD3}},$$

$$\Delta V_{G7\text{-}QD4} = \frac{e}{C_{G7\text{-}QD4} + \frac{C_{M34}}{C_3}C_{G7\text{-}QD3} + (\frac{C_{M24}}{C_2} + \frac{C_{M23}C_{M34}}{C_2C_3})C_{G7\text{-}QD2}}. \quad (11)$$

We take capacitances $C_{G3\text{-}QD1} \approx 4.10$ aF, $C_{G4\text{-}QD2} \approx 8.70$ aF and $C_{G6\text{-}QD3} \approx 6.91$ aF as extracted from the measurements of the two DQDs in Fig. 2 of the main article. Capacitances C_S and C_D are assumed to be equal and are estimated from the charge stability diagram of the single QD in Fig. S1 to be $C_S = C_D \approx 8.00$ aF. Because of the weak coupling between QD2 and QD4 (QD1 and QD3), the associated inter-dot capacitance is small and thus a value of $C_{M24} \approx 0.02$ aF ($C_{M13} \approx 0.02$ aF) is assumed. To extract the remaining capacitances in the QQD device, we consider the measured stability diagram shown in Fig. 3(a) of the main article. From this charge stability diagram, it is found that the individual voltage changes that are required to move from one resonant current line to the next line as a result of resonance transport through individual QDs are $\Delta V_{G3\text{-}QD1} = 0.042$ V, $\Delta V_{G3\text{-}QD2} = 0.083$ V, $\Delta V_{G7\text{-}QD2} = 0.448$ V, $\Delta V_{G3\text{-}QD3} = 0.461$ V, $\Delta V_{G7\text{-}QD3} = 0.034$ V, $\Delta V_{G7\text{-}QD4} = 0.063$ V, $\Delta V_{G7\text{-}QD1} \approx \infty$, and $\Delta V_{G3\text{-}QD4} \approx \infty$. Inserting these voltage change values into Eq. (11) and considering the fact that $C_{i=1,2,3,4} >> C_{Mij}$ (where, on the right side, $i<j$ with $i=1, 2, 3$ and $j=2, 3, 4$), all the remaining capacitance values can be extracted. All the capacitance parameters used to obtain the charge stability diagram of the QQD are listed in Table SI. Figure 4(b) of the main article displays a simulated charge stability diagram of the QQD based on the capacitance network model developed here with the input capacitance values listed in Table SI. It shows a good agreement with our experiment and thus confirm our assignments of the current lines observed in the measured charge stability diagram shown in Fig. 3(a) of the main article.

TABLE SI. Values of the capacitances, in units of aF, used to simulate the charge stability diagram of the nanowire QQD shown in Fig. 3(a) of the main article. The simulated charge stability diagram for the QQD device is shown in Fig. 4(b) of the main article.

$C_{i=S,D}$	C_{M12}	C_{M13}	$C_{G3\text{-}QD1}$	C_{M23}	C_{M24}	$C_{G3\text{-}QD2}$
8.00	0.75	0.02	4.10	0.80	0.02	1.77
$C_{G4\text{-}QD2}$	$C_{G7\text{-}QD2}$	C_{M34}	$C_{G3\text{-}QD3}$	$C_{G6\text{-}QD3}$	$C_{G7\text{-}QD3}$	$C_{G7\text{-}QD4}$
8.70	0.15	1.20	0.30	6.91	4.36	2.26

Based on the capacitance network model and the extracted capacitances listed in Table SI, we also calculate the charge stability diagram of the QQD in the resonance region as shown in Fig. 5(d) of the main article with $V_{G4} = -0.386$ V and $V_{G6} = -1.0535$ V. The results are shown in Fig. S4. Compared to the experimental results shown in Fig. 5(d) of the main article, the spacing between the two current lines corresponding to resonant transport through QD1 and QD2 and the spacing between the current lines corresponding to resonant transport through QD3 and QD4 found in the simulated charge stability diagram are again in good agreement with the experiment. However, at the avoiding crossings of different current lines, the simulated line shapes appear to be clearly different from the experiment ones. These differences are due to the fact that the quantum tunnel coupling mechanism has been neglected in our model simulations.[4,6]

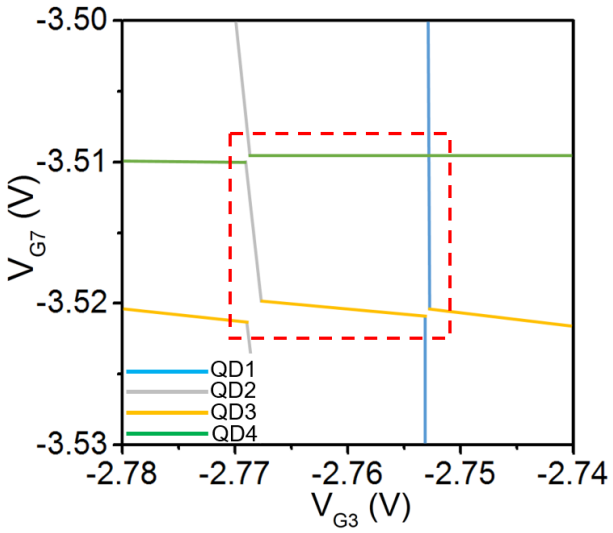

Fig. S4 Calculated charge stability diagram for the nanowire QQD in the resonance region as shown in Fig. 5(d) of the main article with the voltages applied to plunger gates G4 and G6 set at $V_{G4} = -0.386$ V and $V_{G6} = -1.0535$ V, with the values of the capacitances given in Table SI. The blue, grey, yellow, and green lines represent the resonant current lines arising from tunneling via the energy levels of QD1, QD2, QD3, and QD4, respectively.

V. Achieving the resonance between the energy levels of QD3 and QD4 in the QQD device studied in the main article

Figures S5(a) to S5(i) show the source-drain current I_{ds} measured for the QQD device as a function of V_{G3} and V_{G7} (charge stability diagrams) at different voltage values of V_{G6}. Note that Figs. S5(a) and S5(e) are the same figures as Figs. 5(a) and 5(b) of the main article. The current lines marked with grey, yellow and green dash lines in Figs. S5(a) to S5(i) arise from resonant

transport via the energy levels in QD2, QD3 and QD4, respectively. Figures S5(a) to S5(i) demonstrate that with decreasing V_{G6}, the spacing between a current line (labeled by 3) corresponding to resonant transport through the energy level of QD3 and a current line (labeled by 4) corresponding to resonant transport through the energy level of QD4 decreases, reaches a minimum at $V_{G6} = -1.0535$ V, and then increases. Thus, it is achieved that at $V_{G6} = -1.0535$ V, the energy levels of QD3 and QD4 are found to be on resonance with each other.

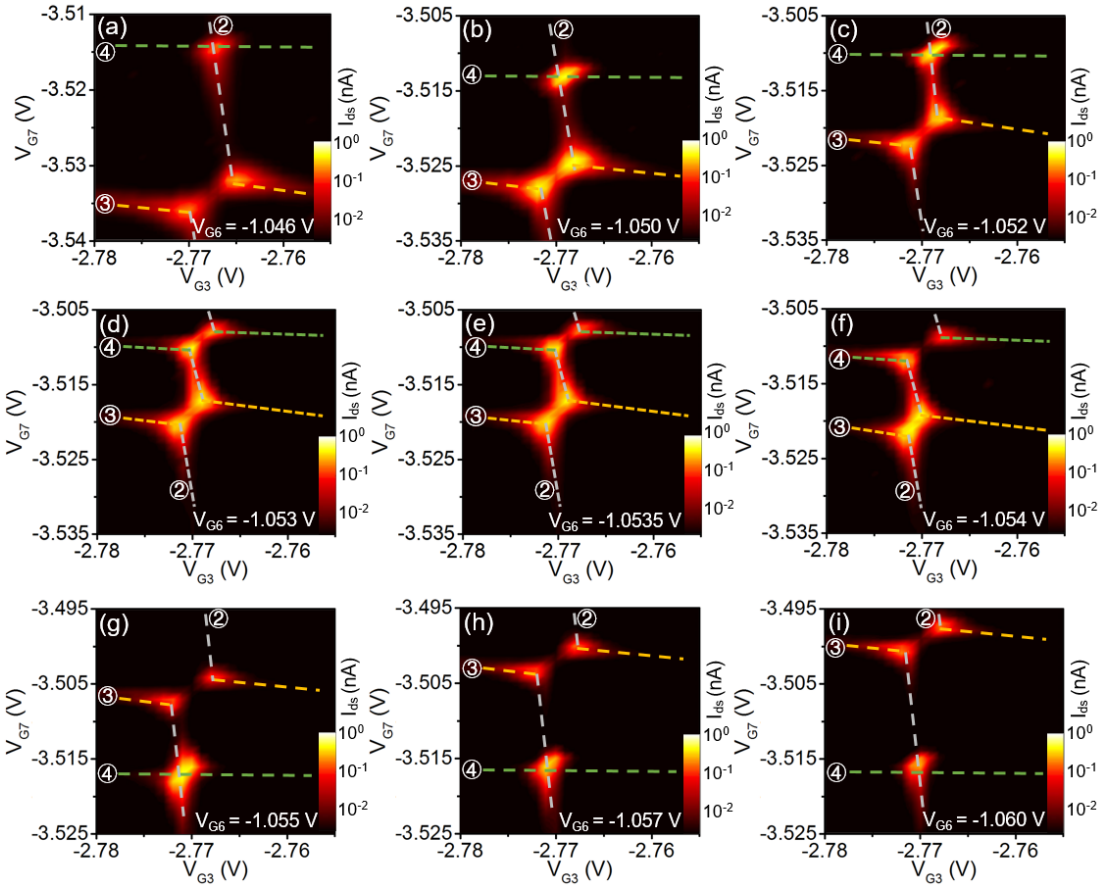

Fig. S5 Charge stability diagrams measured for the QQD device at (a) $V_{G6} = -1.046$ V, (b) $V_{G6} = -1.050$ V, (c) $V_{G6} = -1.052$ V, (d) $V_{G6} = -1.053$ V, (e) $V_{G6} = -1.0535$ V, (f) $V_{G6} = -1.054$ V, (g) $V_{G6} = -1.055$ V, (h) $V_{G6} = -1.057$ V, and (i) $V_{G6} = -1.060$ V. The measurements are performed with the barrier gate voltages set at $V_{G1} = -2.55$ V, $V_{G5} = -3.35$ V and $V_{G9} = -3.855$ V, and the plunger gate voltages set at $V_{G4} = -0.384$ V and $V_{G8} = -0.94$ V. The source-drain voltage is set at $V_{ds} = 0.2$ mV in (a) and (b), and at $V_{ds} = 40$ μV in the other seven panels. The current lines marked by the grey, yellow and green dashed lines arise from resonant transport through QD2, QD3 and QD4, respectively. These current lines are also labeled by the corresponding QD numbers 2, 3 and 4.

References

1 I. Shorubalko, R. Leturcq, A. Pfund, D. Tyndall, R. Krischek, S. Schön and K. Ensslin, *Nano Lett.*, 2008, **8**, 382–385.

2 W. G. Van der Wiel, S. De Franceschi, J. M. Elzerman, T. Fujisawa, S. Tarucha and L. P. Kouwenhoven, *Rev. Mod. Phys.*, 2002, **75**, 1-22.

3 L. Gaudreau, S. A. Studenikin, A. S. Sachrajda, P. Zawadzki, A. Kam, J. Lapointe, M. Korkusinski and P. Hawrylak, *Phys. Rev. Lett.*, 2006, **97**, 036807.

4 D. Schröer, A. D. Greentree, L. Gaudreau, K. Eberl, L. C. L. Hollenberg, J. P. Kotthaus and S. Ludwig, *Phys. Rev. B*, 2007, **76**, 075306.

5 J. Y. Wang, S. Huang, G. Y. Huang, D. Pan, J. Zhao and H. Q. Xu, *Nano Lett.*, 2017, **17**, 4158-4164.

6 C. B. Simmons, M. Thalakulam, B. M. Rosemeyer, B. J. Van Bael, E. K. Sackmann, D. K. Savage, M. G. Lagally, R. Joynt, M. Friesen and S. N. Coppersmith, *Nano Lett.*, 2009, **9**, 3234-3238.